Mineralogy and Petrology (2002) 75: 131–152

Mineralogy and Petrology

© Springer-Verlag 2002
Printed in Austria

Experimental melting of a modally heterogeneous mantle

V. K. Bulatov[1], **A. V. Girnis**[2], and **G. P. Brey**[3]

[1] Vernadsky Institute of Geochemistry and Analytical Chemistry, Russian Academy of Sciences, Moscow, Russia
[2] Institute of the Geology of Ore Deposits, Petrography, Mineralogy and Geochemistry, Russian Academy of Sciences, Moscow, Russia
[3] Institut für Mineralogie, J. W. Goethe-Universität Frankfurt, Frankfurt/M, Federal Republic of Germany

With 5 Figures

Received October 10, 2000;
revised version accepted August 31, 2001

Summary

Melting of a spinel lherzolite with a spinel clinopyroxenite layer was investigated experimentally from 3.5 to 20 kbar and from 1200 to 1450 °C. The melt fraction in the spinel pyroxenite layer increases rapidly, and clinopyroxene disappears leaving olivine-spinel residua according to the reaction $Cpx + Sp = Ol + Liq$. The melt in the pyroxenite layer reacts with the surrounding lherzolite resulting in the formation of an essentially monomineral (olivine) zone with interstitial melt near the former pyroxenite. Melt compositions in the central melt pool are similar to those produced by other authors in melting experiments with peridotites similar to the bulk compositions of our samples. It is suggested that similar small-scale mantle heterogeneities (i.e. thin pyroxenite layers in lherzolite) may exert significant influence on mantle rheology and melt segregation, whereas melt compositions are not strongly affected and controlled by the dominating lherzolite lithology.

Introduction

Considerable experimental work has been dedicated to equilibrium melting of mantle peridotite and generation of primary basalt magmas (*Ito* and *Kennedy*, 1967; *Jaques* and *Green*, 1980; *Stolper*, 1980; *Sen*, 1982; *Takahashi* and *Kushiro*, 1983; *Fujii* and *Scarfe*, 1985; *Falloon* and *Green*, 1987, 1988). Recent studies demonstrated the complex nature of initial magmas (e.g. *Langmuir* et al., 1977, 1992; *O'Hara*, 1985; *Plank* and *Langmuir*, 1992) including polybaric melting and mixing of melts from different mantle zones and lithologies. There is increasing

evidence on the heterogeneity on various scales in the source regions of mid-ocean ridge and oceanic island basalt. Peridotite xenoliths and massifs often contain veins and zones of pyroxene-rich rocks including pyroxenite and eclogite (*Irving*, 1980; *Sautter* and *Fabries*, 1990; *Jackson* and *Wright*, 1970; *Kornprobst*, 1969; *Bodiner* et al., 1987; *Kumar* et al., 1996). These veins are usually 1–10 cm, occasionally up to 2 m thick. They could be formed either by recycling and stretching of oceanic crust (*Allegre* and *Turcotte*, 1986; *Kellogg* and *Turcotte*, 1990) or crystal segregation along magma conduits in the mantle (*Kornprobst*, 1969; *Irving*, 1980; *Bodiner* et al., 1987; *Kumar* et al., 1996). Smaller scale mantle heterogeneity includes millimetre-sized patches and lenses of spinel or plagioclase pyroxenites, which might represent crystallised melts (e.g. *Jousselin* and *Mainprice*, 1998). Heterogeneities on a similar scale are found in sheared mantle xenoliths, where they could form below the mantle solidus in response to deformation (e.g. *Witt* and *Seck*, 1987).

Melting of such heterogeneous material will differ from that of homogeneous lherzolite, and certain features of oceanic magmatism can be explained in this way. *Hirschmann* and *Stolper* (1996) discussed the possible role of pyroxenite zones (veins) in mantle lherzolite for the genesis of mid-ocean ridge basalts. Melting of an inhomogeneous mantle was also considered to be crucial for the origin of Hawaiian magmas (e.g. *Sen*, 1988; *Yang* et al., 1998). The solidus of clinopyroxenite or eclogite may be lower than that of lherzolite (pyrolite) (*Campbell*, 1998), whereby the experimental evidence on pyroxenite melting is limited and the dependency on clinopyroxene composition is not adequately known. Another important process is the interactions of the melt formed in the pyroxene-rich zones with the enclosing lherzolitic or harzburgitic material. In order to study this process in more detail we undertook experimental melting of layered lherzolite/spinel pyroxenite samples at pressures from 3.5 to 20 kbar.

Experimental methods

Sample configuration (Fig. 1) was similar to that used in the basalt-peridotite sandwich experiments (e.g. *Stolper*, 1980). Samples consisted of a clinopyroxene-spinel disk, 2 mm in diameter and 0.5 mm high, surrounded by an olivine-orthopyroxene-clinopyroxene-spinel matrix. The disk and matrix were pressed from

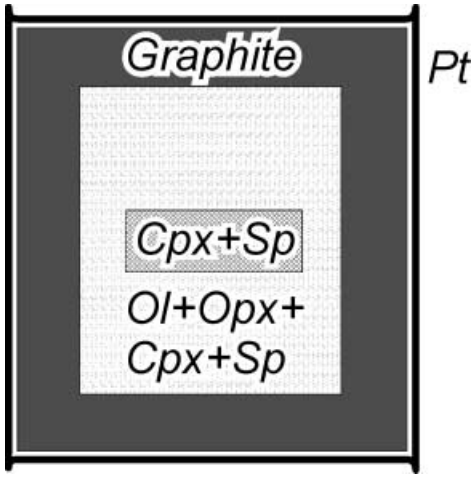

Fig. 1. Schematic drawing of the experimental setup

powdered (<10 μm grain size) mixtures of natural mineral separates. The bulk composition of samples corresponded to the compositions of the lherzolites studied.

The sample was placed in a graphite container, 4 mm o.d. and 4.5 mm high, loaded in a platinum tube, 4.2 mm o.d., and stored at 120 °C for at least 24 hours before welding. The capsule was pressed (peridotite sample was approximately 3 mm long after this procedure) and placed into a CaF_2-based graphite furnace assembly (*Bulatov*, 1990).

The graphite-Pt capsule assembly keeps oxygen fugacity near the C–CO–CO_2 (CCO) buffer, i.e. within the wüstite stability field (*Thompson* and *Kushiro*, 1972) at 1200–1500 °C and 1.0–2.0 GPa in the presence of a fluid phase. Since no gas phase occurred in our experiments, oxygen fugacity must be lower than C–CO–CO_2 (*Holloway* et al., 1992). The absence of a metal phase (Fe–Ni alloy) constrains oxygen fugacity to be not much lower than the iron-wüstite buffer.

Although the experiments were nominally anhydrous, it is possible that a small amount of H_2O (0.5–1.0 wt.%) was present in the melts (cf. *Fallon* and *Danyushevsky*, 2000). This is suggested by systematically higher temperatures calculated for olivine-liquid equilibrium using empirical relationships (e.g. *Ford* et al., 1983) compared with the experimental temperatures. The discrepancy is about 20–30 °C and increases slightly with decreasing melt fraction.

The experiments were carried out in the Laboratory of Experimental Mineralogy of the Institute of Lithosphere, Russian Academy of Sciences (Moscow), in a half-inch piston-cylinder apparatus, using hot ''piston-in'' technique. No friction correction was applied in the experiments at 10, 15, and 20 kbar. Pressures of 3.5 and 7.5 kbar corresponded to nominal pressures of 5 and 8 kbar, respectively, according to *Bulatov* (1990). Temperature was measured by a $Pt_{70}Rh_{30}$-$Pt_{94}Rh_6$ thermocouple (0.3 mm in diameter) without any emf pressure correction. Temperatures are estimated to be accurate within ± 15° including uncertainties resulting from the temperature gradient and heater deformation, which differed from run to run (*Bulatov*, 1990).

After quenching the charges were sectioned lengthwise with a diamond saw. Thin sections were prepared for optical microprobe studies. Microprobe analyses were carried out in the Geological Department of Gutenberg University (Mainz) with a ''Camebax'' electron probe equipped with a ''Kevex'' energy-dispersive system. Analytical procedures followed those of *Reed* and *Ware* (1975). Accelerating voltage was 20 kV, sample current 20 nA and counting time 100 sec. The glasses were scanned with a focused beam over a square usually of 50 μm × 50 μm or 25 μm × 25 μm and rarely 12 μm × 12 μm to prevent loss of sodium. Minerals were analysed with a focused beam.

Microprobe analyses (5–6 points) of the glass were usually done more than 30 μm from crystalline phases to avoid quench effects (*Nielsen* et al., 1992). The variation of the measurements was within 1% rel. for SiO_2, 2–3% rel. for Al_2O_3, MgO, FeO, and CaO and 0.1 wt.% for Na_2O, Cr_2O_3, and TiO_2, in the range of the analytical error. The larger uncertainties in Na_2O, Cr_2O_3 and TiO_2 are due to their low absolute concentrations. The totals of glass and mineral analyses varied within 98.5–100.5 wt.%.

Complete equilibrium between a central layer and peridotite matrix in sandwich or diamond trap experiments is not attained as indicated by mineral zoning (*Takahashi* and *Kushiro*, 1983; *Falloon* and *Green*, 1987). However, local

equilibrium, i.e. melt saturation with respect to the outer zones of peridotite minerals can be attained within 24 hrs (*Takahashi* and *Kushiro*, 1983; *Fujii* and *Scarfe*, 1985; *Falloon* and *Green*, 1987; *Johnson* and *Kushiro*, 1992; *Hirose* and *Kushiro*, 1993; *Baker* and *Stolper*, 1994). Run times were variable depending on temperature (Table 1) but at maximum possible length allowed by thermocouple degradation. We also performed time studies at 7.5 kbar and 1290–1340 °C with duration ranging from 11 to 63 hrs (Table 2). Central glass layer and olivine compositions do not change anymore after 45 hrs (1290, 1300 °C) or 11 hrs (1325 and 1340 °C).

Table 1. *Experimental conditions and run products*

Run	P, kbar	T °C	Duration, hrs	Run products
		Sample 79/1 (Series A)		
A-20	3.5	1200	70	Gl*,Ol,Opx,Cpx,Pl,Sp
A-32	3.5	1215	70	Gl*,Ol,Sp,Opx,Cpx
A-21	3.5	1225	68	Gl,Ol,Sp,Opx
A-33	3.5	1240	68	Gl,Ol,Sp,Opx
A-22	3.5	1250	68	Gl,Ol,Sp,Opx
A-23	3.5	1275	47	Gl,Ol,Sp,Opx
A-24	3.5	1300	47	Gl,Ol,Sp,Opx
A-43	3.5	1325	48	Gl,Ol,Sp
A-47	7.5	1250	69	Gl*,Ol,Cpx,Sp,Opx
A-49	7.5	1265	71	Gl,OL,Sp,Opx
A-27	7.5	1290	68	Gl,Ol,Sp,Opx
A-28	7.5	1300	45	Gl,Ol,Sp,Opx
A-29	7.5	1325	24	Gl,Ol,Sp,Opx
A-45	7.5	1340	46	Gl,Ol,Sp,Opx
A-30	7.5	1350	24	Gl,Ol,Sp,Opx
A-44	7.5	1385	22	Gl,Ol,Sp
A-31	7.5	1400	24	Gl,Ol
A-6	10	1260	66	Gl*,Ol,Opx,Cpx,Sp
A-39	10	1275	67	Gl,Ol,Opx,Cpx,Sp
A-7	10	1290	66	Gl,Ol,Opx,Cpx,Sp
A-8	10	1315	68	Gl,Ol,Opx,Sp
A-9	10	1325	22	Gl,Ol,Opx,Sp
A-10	10	1340	24	Gl,Ol,Opx,Sp
A-11	10	1375	22	Gl,Ol,Opx,Sp
A-48	10	1420	22	Gl,Ol,Opx
A-12	15	1325	43	Gl*,Ol,Opx,Cpx,Sp
A-13	15	1350	24	Gl*,Ol,Opx,Cpx,Sp
A-14	15	1375	24	Gl,Ol,Opx,Sp
A-15	15	1400	23	Gl,Ol,Opx,Sp
A-16	15	1425	22	Gl,Ol,Opx
A-51	15	1450	22	Gl,Ol,Opx
A-17	20	1415	22	Gl*,Ol,Opx,Cpx,Sp
A-18	20	1440	22	Gl,Ol,Sp,Opx
A-19	20	1465	22	Gl,Ol,Opx

(*continued*)

Table 1 (*continued*)

Run	P, kbar	T °C	Duration, hrs	Run products
		Sample ShT-1 (Series B)		
B-37	7.5	1260	68	Gl*,Ol,Cpx,Sp,Opx
B-31	7.5	1280	68	Gl,Ol,Sp,Opx
B-8	7.5	1300	48	Gl,Ol,Sp,Opx
B-9	7.5	1310	46	Gl,Ol,Sp,Opx
B-32	7.5	1325	46	Gl,Ol,Sp,Opx
B-11	7.5	1350	22	Gl,Ol
B-15	10	1285	48	Gl*,Ol,Cpx,Sp,Opx
B-38	10	1300	46	Gl*,Ol,Cpx,Sp,Opx
B-34	10	1330	46	Gl,Ol,Sp,Opx
B-17	10	1350	24	Gl,Ol,Sp,Opx
B-36	10	1375	23	Gl,Ol,Opx
B-21	15	1350	23	Gl*,Ol,Cpx,Sp,Opx
B-22	15	1375	24	Gl*,Ol,Cpx,Sp,Opx
B-23	15	1400	23	Gl,Ol,Opx

Phase abbreviation: *Gl* glass, *Ol* olivine, *Sp* spinel, *Pl* plagioclase, *Opx* orthopyroxene, *Cpx* clinopyroxene, *Gl** interstitial glass

Table 2. *Comparison of melt and mineral compositions in kinetic experiments with varying duration at 7.5 kbar*

T °C	1290		1300		1325		1340	
Duration hrs.	46	68	45	67	11	24	11	46
				Glass composition				
SiO_2	50.8	50.3	50.5	50.7	50.6	50.7	51.1	50.7
TiO_2	0.4	0.4	0.4	0.4	0.4	0.3	0.3	0.3
Al_2O_3	15.2	15.4	15	14.7	14	14.2	13.3	13.5
Cr_2O_3	0.3	0.3	0.4	0.3	0.4	0.4	0.5	0.5
FeO	7.3	7.4	7.5	7.7	8	8	8.3	8.3
MgO	12.7	12.9	13.2	13.2	14.8	14.4	15.3	15.3
CaO	11.9	11.8	11.6	11.7	10.6	10.7	10.1	10.2
Na_2O	1.4	1.5	1.4	1.3	1.2	1.3	1.1	1.2
mg	0.756	0.757	0.758	0.754	0.767	0.763	0.767	0.767
mg_{Ol}	0.907	0.908	0.908	0.905	0.907	0.909	0.91	0.91
				Spinel compositions				
SiO_2	0.25	0.15	0.13	0	0	0	0	0
TiO_2	0.3	0.21	0.14	0.19	0.15	0.16	0.23	0
Al_2O_3	32.74	32.43	31.54	30.35	29.53	29.75	24.37	25.81
Cr_2O_3	37.56	38.65	40	41.23	42.05	41.75	47.73	46.61
FeO	10.19	10.16	10.11	10.32	10.2	10.23	10.44	10.51
MgO	17.92	17.85	17.8	17.43	17.69	17.93	16.72	16.74
CaO	0.27	0.17	0	0.15	0.13	0	0.2	0
mg	0.758	0.758	0.758	0.751	0.755	0.757	0.74	0.74

mg Mg/(Mg + Fe). All analyses are recalculated to a total of 100 wt.%

Starting materials

Minerals were separated from two spinel lherzolite xenoliths, Samples 79/1 (Series A experiments) and ShT-1 (Series B experiments) (Table 3), which were collected by D. I. Ionov and V. I. Kovalenko from the eruptive centre of Shavaryn-Tsaram Volcano (Tariat Depression, Mongolia). The compositions of the spinel lherzolites correspond to slightly depleted upper mantle material (*Press* et al., 1986; *Igneous Rocks*, 1988). Minerals were hand-picked under a binocular microscope and washed in 2 N HCl.

Table 3. *Compositions of peridotites and their minerals (wt.%) used as starting materials in the experiments*

	Ol	Opx	Cpx	Sp	Lherz*	Pyrox**	Bulk***
			Series A, spinel lherzolite Sample 79/1				
SiO_2	40.45	54.82	52.79	–	44.53	43.29	44.45
TiO_2	–	–	0.47	0.15	0.04	0.41	0.07
Al_2O_3	–	4.88	7.13	57.88	3.08	16.26	4.08
Cr_2O_3	–	0.1	0.63	9.33	0.27	2.2	0.41
FeO	10.5	6.58	3.15	11.12	8.82	4.58	8.5
MnO	0.14	0.19	–	–	0.14	–	0.13
NiO	0.27	–	–	0.37	0.18	0.07	0.17
MgO	48.64	32.48	14.75	21.15	40.81	15.9	38.9
CaO	–	0.7	19.28	–	1.9	15.81	2.97
Na_2O	–	0.25	1.8	–	0.23	1.48	0.32
			Series B, spinel lherzolite Sample ShT-1				
SiO_2	40.27	55.37	52.97	–	44.9	45.77	44.96
TiO_2	–	–	0.44	–	0.06	0.38	0.08
Al_2O_3	–	4.09	6.9	60.1	3.21	14.13	4.05
Cr_2O_3	–	0.18	0.51	7.7	0.27	1.49	0.37
FeO	10.72	6.86	2.74	10.65	8.69	3.82	8.31
MnO	0.21	0.24	–	–	0.18	–	0.17
NiO	0.34	–	–	0.43	0.21	0.06	0.2
MgO	48.46	32.6	14.13	21.12	39.33	15.08	37.47
CaO	–	0.45	20.28	–	2.83	17.52	3.96
Na_2O	–	0.21	2.03	–	0.32	1.75	0.43

Minerals were analyzed on an electron microprobe in Gutenberg University (Mainz). Compositions are recalculated to totals of 100 wt.%

*Composition of Ol + Opx + Cpx + Sp matrix calculated from mineral compositions and proportions:
Series A: 0.627Ol + 0.264Opx + 0.089Cpx + 0.02Sp;
Series B: 0.596Ol + 0.249Opx + 0.134Cpx + 0.02Sp

**Composition of Cpx + Sp aggregate in central disks calculated from mineral compositions and proportions:
Series A: 0.82Cpx + 0.18Sp;
Series B: 0.864Cpx + 0.136Sp

***Bulk compositions of samples calculated from compositions and weight proportions of lherzolite and pyroxenite parts

Lherzolite 79/1 is slightly more depleted than ShT-1 corresponding to lower modal Cpx and lower CaO, Na_2O, SiO_2 and higher MgO and FeO in the bulk. Chemical compositions of the matrix, the Cpx-Sp layer, and the bulk of the experimental samples are calculated from the proportions of minerals used (Table 3). The bulk sample (lherzolite matrix + pyroxenite) is similar to the lherzolite compositions used in experiments by *Hirose* and *Kushiro* (1993), *Baker* and *Stolper* (1994) and *Baker* et al. (1995), which will be discussed later.

Experimental results

Compositions of experimentally produced glasses and mineral phases are given in Table 4.

Melting in both series and at all pressures follows a similar pattern explained here for Series A experiments at 10 kbar (Fig. 2).

1260 °C. First evidence of melting is observed in the lherzolite matrix as uniformly distributed thin films and pockets; the central layer contains clinopyroxene, spinel and newly-formed olivine and melt, distributed uniformly.

1290 °C. Three zones can be distinguished – a central zone with an upper clear glass (melt) layer and a lower layer of accumulated olivine and spinel with interstitial glass. No clinopyroxene was found in this central zone. This zone is surrounded by coarse-grained olivine + interstitial melt only with a thickness of about 0.5 mm (lighter part). The outermost part (matrix) consists of lherzolite (Ol + Opx + Cpx) with a small amount of interstitial melt (smaller than in the reaction zone). The boundary between the lherzolite and the olivine reaction zone is sharp (Fig. 3).

1315 °C. The layer of glass in the central zone has increased and comprises more than 50 vol.%. The lower part again consists of accumulated olivine and spinel with interstitial melt. The olivine reaction zone is similar as before, but clinopyroxene was not found in the outer lherzolite zone.

1325 °C. The relationships are essentially the same as at 1315 °C. Melt fraction increases in all zones.

1340 °C. Deformation of the central layer is observed first at this temperature with upper and lower boundaries becoming concave. The cumulate layer in the central zone is dominated by spinel.

1375 °C. Mineral relationships in all zones are the same as in the previous experiments. The deformation of the central layer continues and the melt is squeezed out into the reaction zone. Small melt pools remain and spinel traces the former pyroxenite layer.

1420 °C. Spinel is completely dissolved in the central zone. No separate melt pools are observed and the sample is composed of a central melt + olivine and an outer melt + olivine + orthopyroxene zone.

Composition of melts

It was not possible to analyse melts in the lherzolite matrix and in the reaction zone near the pyroxenite layer; all melt composition data are for the large melt pools in the central zones. The isobaric temperature dependencies of melt compositions are

Table 4. *Microprobe analyses (wt%) of experimental phases*

Run, P(kb), T °C	Phase	SiO_2	TiO_2	Al_2O_3	Cr_2O_3	FeO	MnO	MgO	CaO	Na_2O	NiO	V_2O_3	F	mg	Kd
A-20, 3.5, 1200	Ol	40.34	–	0.17	–	10.35	–	48.66	0.16	–	0.32	–		0.893	
	Cpx	52.48	0.32	5.99	0.98	3.33	–	15.55	20.12	1.23	–	–		0.893	
	Opx	54.76	–	5.00	0.38	6.73	–	32.36	0.67	0.10	–	–		0.896	
	Pl	45.76	–	34.71	–	–	–	0.14	18.08	1.31	–	–			
	Sp	–	0.48	46.27	22.80	11.48	–	18.80	–	–	–	0.17		0.745	
A-32, 3.5, 1215	Gl	51.3	0.6	16.8	0.2	6.5	–	9.8	13.3	1.5	–	–	21.3	0.729	
	Ol	40.44	–	0.14	0.33	9.60	–	49.22	0.26	–	–	–		0.901	0.294
	Sp	–	0.19	33.24	38.41	10.21	–	17.52	0.11	–	–	0.32		0.754	0.879
A-21, 3.5, 1225	Gl	51.4	0.5	16.7	0.2	6.5	–	10.4	12.9	1.4	–	–	22.8	0.740	
	Ol	40.44	–	–	0.23	9.49	–	49.35	0.20	–	0.29	–		0.903	0.308
	Sp	–	0.18	34.70	36.38	9.96	–	18.47	–	–	–	0.32		0.768	0.863
A-33, 3.5, 1240	Gl	51.6	0.5	16.3	0.3	6.8	–	11.0	12.2	1.3	–	–	24.6	0.743	
	Ol	40.66	–	–	0.23	9.49	–	49.35	0.20	–	0.29	–		0.903	0.311
	Sp	–	0.22	31.36	40.18	10.55	–	17.22	–	–	–	0.47		0.744	0.991
A-22, 3.5, 1250	Gl	51.9	0.4	15.8	0.3	6.9	–	11.8	11.6	1.3	–	–	24.6	0.753	
	Ol	40.59	–	0.18	0.33	8.87	–	49.65	0.16	–	0.22	–		0.909	0.306
	Sp	–	0.24	30.01	41.42	10.28	–	17.48	0.21	–	–	0.28		0.752	1.006
A-23, 3.5, 1275	Gl	51.9	0.4	14.9	0.4	7.3	–	13.1	10.8	1.2	–	–	26.7	0.762	
	Ol	40.51	–	0.21	0.45	8.66	–	49.77	0.17	–	0.24	–		0.911	0.312
	Sp	0.13	0.21	28.27	43.50	10.13	–	17.35	0.12	–	–	0.29		0.753	1.048
A-24, 3.5, 1300	Gl	52.1	0.4	14.0	0.5	7.7	–	13.9	10.3	1.1	–	–	29	0.763	
	Ol	40.84	–	–	0.35	8.57	–	50.05	0.19	–	–	–		0.912	0.309
	Sp	–	0.16	24.67	47.01	10.33	0.39	16.97	0.18	–	–	0.29		0.745	1.099
A-43, 3.5, 1325	Gl	52.3	0.3	12.9	0.7	8.3	–	15.1	9.4	1.0	–	–	32	0.764	
	Ol	40.79	–	–	0.52	8.24	–	50.45	–	–	–	–		0.916	0.297
	Sp	–	0.16	18.99	54.32	9.95	–	16.07	0.13	–	–	0.37		0.742	1.126
A-47, 7.5, 1250	Gl	49.9	0.5	17.1	0.2	6.9	–	10.6	13.0	1.8	–	–	17.8	0.733	
	Ol	40.42	–	0.25	0.14	9.89	–	48.81	0.20	–	0.28	–		0.898	0.311
	Cpx	52.16	0.37	6.30	0.88	3.20	–	16.74	19.10	1.25	–	–		0.903	0.294
	Sp	–	–	43.71	26.46	9.81	–	19.85	–	–	–	0.17		0.783	0.759

(*continued*)

Table 4 (*continued*)

Run, P(kb), T °C	Phase	SiO_2	TiO_2	Al_2O_3	Cr_2O_3	FeO	MnO	MgO	CaO	Na_2O	NiO	V_2O_3	F	mg	Kd
A-49, 7.5, 1265	Gl	50.1	0.4	16.5	0.2	7.0	–	11.4	12.7	1.7	–	–	18.8	0.744	
	Ol	40.72	–	–	–	9.24	–	49.50	0.28	–	0.26	–		0.905	0.304
	Sp	0.16	–	40.49	29.96	9.85	–	19.28	–	–	0.27	–		0.777	0.832
A-27, 7.5, 1290	Gl	50.3	0.4	15.4	0.3	7.4	–	12.9	11.8	1.5	–	–	21.3	0.757	
	Ol	40.66	–	0.14	0.31	8.91	–	49.69	0.29	–	–	–		0.909	0.313
	Sp	0.15	0.21	32.43	38.65	10.16	–	17.85	0.17	–	–	0.38		0.758	0.992
A-28, 7.5, 1300	Gl	50.5	0.4	15.0	0.4	7.5	–	13.2	11.6	1.4	–	–	22.9	0.758	
	Ol	40.69	–	0.19	0.34	8.94	–	49.64	0.20	–	–	–		0.908	0.317
	Sp	0.13	0.14	31.54	40.00	10.11	–	17.80	–	–	–	0.28		0.758	1.000
A-29, 7.5, 1325	Gl	50.7	0.3	14.2	0.4	8.0	–	14.4	10.7	1.3	–	–	24.6	0.762	
	Ol	40.66	–	0.19	0.33	8.91	–	49.77	0.14	–	–	–		0.909	0.322
	Sp	–	0.16	29.75	41.75	10.23	–	17.93	–	–	–	0.19		0.758	1.027
A-45, 7.5, 1340	Gl	50.7	0.3	13.5	0.5	8.3	–	15.3	10.2	1.2	–	–	26.6	0.767	
	Ol	40.60	–	0.20	0.64	8.79	–	49.62	0.14	–	–	–		0.910	0.327
	Sp	–	–	25.81	46.61	10.51	–	16.74	–	–	–	0.34		0.740	1.157
A-30, 7.5, 1350	Gl	51.0	0.3	13.2	0.5	8.2	–	15.7	10.0	1.1	–	–	29.1	0.773	
	Ol	40.54	–	0.21	0.32	8.58	–	50.25	0.11	–	–	–		0.913	0.327
	Sp	0.30	0.17	24.50	47.35	10.26	–	16.97	0.16	–	–	0.30		0.747	1.158
A-44, 7.5, 1385	Gl	51.3	0.2	11.7	0.5	8.8	–	18.0	8.6	0.9	–	–	35.5	0.785	
	Ol	40.76	–	–	0.46	8.23	–	50.54	–	–	–	–		0.916	0.333
	Sp	0.16	0.21	20.20	52.61	9.97	–	16.55	0.10	–	–	0.20		0.747	1.232
A-31, 7.5, 1400	Gl	51.2	0.2	11.3	0.5	9.1	–	18.6	8.2	0.9	–	–	35.5	0.785	
	Ol	40.80	–	–	0.38	8.17	–	50.65	–	–	–	–		0.917	0.330
A-6, 10, 1260	Gl*	49.2	0.6	17.7	0.2	6.9	–	10.6	12.5	2.5	–	–	12.7	0.733	
	Ol	40.51	–	–	–	10.16	0.10	48.80	0.17	–	0.26	–		0.895	0.320
	Cpx	51.36	0.30	7.10	0.84	3.50	–	16.40	19.60	0.90	–	–		0.893	0.328
	Opx	54.79	–	5.12	0.30	6.75	–	32.04	0.70	0.30	–	–		0.894	0.324
	Sp	0.38	0.21	56.10	12.71	8.43	–	21.72	–	–	0.26	0.18		0.821	0.597
A-39, 10, 1275	Gl	49.3	0.6	16.8	0.2	7.1	–	11.4	12.8	1.8	–	–	17.7	0.741	
	Ol	40.74	–	–	–	9.81	–	49.03	0.18	–	0.24	–		0.899	0.321
	Cpx	51.45	–	6.80	1.07	3.63	–	18.05	18.50	0.50	–	–		0.899	0.323
	Opx	54.68	–	5.02	0.61	6.35	–	31.72	1.60	0.20	–	–		0.899	0.321
	Sp	–	–	51.20	18.58	9.48	–	20.73	–	–	–	–		0.796	0.734

(*continued*)

Table 4 (*continued*)

Run, P(kb), T °C	Phase	SiO_2	TiO_2	Al_2O_3	Cr_2O_3	FeO	MnO	MgO	CaO	Na_2O	NiO	V_2O_3	F	mg	Kd
A-7, 10, 1290	Gl	49.5	0.5	16.1	0.2	7.2	–	12.2	12.7	1.6	–	–	20	0.751	
	Ol	40.55	–	0.15	0.22	9.50	–	49.44	0.14	–	–	–		0.903	0.326
	Cpx	51.82	–	6.36	1.35	3.52	–	18.80	17.75	0.40	–	–		0.905	0.317
	Opx	54.83	–	4.28	1.03	5.93	–	31.58	2.20	0.15	–	–		0.905	0.318
	Sp	0.16	–	41.93	28.38	9.61	–	19.71	–	–	–	0.22		0.785	0.826
A-8, 10, 1315	Gl	49.7	0.4	15.2	0.3	7.5	–	13.3	12.1	1.5	–	–	21.3	0.760	
	Ol	40.66	–	0.10	0.26	9.13	–	49.72	0.13	–	–	–		0.907	0.377
	Opx	55.22	0.13	3.85	1.05	5.94	–	31.94	1.87	–	–	–		0.906	0.381
	Sp	0.16	–	34.44	36.57	9.89	–	18.49	–	–	0.27	0.18		0.769	1.097
A-9, 10, 1325	Gl	49.9	0.4	14.6	0.4	7.8	–	14.2	11.3	1.4	–	–	22.9	0.764	
	Ol	40.62	–	0.19	0.39	8.83	–	49.49	0.25	–	0.23	–		0.909	0.334
	Opx**	55.37	–	4.44	0.46	6.25	–	32.70	0.78	–	–	–		0.903	0.357
	Sp	0.41	0.21	32.18	38.72	10.03	–	18.07	0.15	–	–	0.22		0.763	1.038
A-10, 10, 1340	Gl	50.0	0.3	14.2	0.4	8.0	–	15.0	10.8	1.3	–	–	24.6	0.770	
	Ol	40.89	–	–	0.22	8.85	–	49.94	0.10	–	–	–		0.910	0.319
	Opx	55.55	–	3.31	1.08	5.70	–	32.70	1.66	–	–	–		0.911	0.314
	Sp	0.17	–	30.64	41.08	9.94	–	18.18	–	–	–	–		0.765	0.985
A-11, 10, 1375	Gl	50.4	0.3	12.8	0.6	8.3	–	17.0	9.5	1.1	–	–	29	0.785	
	Ol	40.93	–	–	0.42	8.09	–	50.56	–	–	–	–		0.918	0.293
	Opx	55.97	–	2.91	1.09	5.21	–	33.53	1.29	–	–	–		0.920	0.284
	Sp	0.20	0.28	23.59	48.49	9.65	0.35	17.11	–	–	–	0.33		0.760	1.032
A-48, 10, 1420	Gl	50.7	0.3	11.5	0.7	9.0	–	18.4	8.5	0.9	–	–	35.5	0.785	
	Ol	41.01	–	–	0.41	8.15	–	50.17	–	–	0.26	–		0.916	0.288
A-12, 15, 1325	Gl*	48.0	0.8	16.5	0.2	7.7	–	12.5	11.7	2.6	–	–	12.5	0.743	
	Ol	40.42	–	–	–	10.00	–	49.07	0.19	–	0.22	–		0.897	0.330
	Cpx	51.12	0.10	8.07	1.16	3.57	–	17.95	17.26	0.77	–	–		0.900	0.322
	Opx	54.10	–	5.70	0.50	6.30	–	31.50	1.65	0.25	–	–		0.899	0.324
	Sp	0.26	–	57.43	11.03	8.39	–	22.41	0.19	–	0.29	–		0.826	0.607
A-13, 15, 1350	Gl*	48.3	0.4	15.4	0.3	8.0	–	14.0	12.1	1.5	–	–	21	0.756	
	Ol	40.72	–	–	0.20	9.32	0.15	49.20	0.16	–	0.25	–		0.904	0.330
	Cpx	51.58	–	7.28	1.20	3.75	–	19.55	15.94	0.70	–	–		0.903	0.334
	Opx	54.40	–	5.40	0.60	5.90	–	31.20	2.30	0.20	–	–		0.904	0.330
	Sp	0.18	–	50.74	18.55	8.84	–	21.45	–	–	0.24	–		0.812	0.718

(*continued*)

Table 4 (*continued*)

Run, P(kb), T °C	Phase	SiO_2	TiO_2	Al_2O_3	Cr_2O_3	FeO	MnO	MgO	CaO	Na_2O	NiO	V_2O_3	F	mg	Kd
A-14, 15, 1375	Gl	48.8	0.3	14.3	0.3	8.3	–	15.3	11.3	1.4	–	–	22.8	0.767	
	Ol	40.72	–	–	0.30	9.04	–	49.51	0.20	–	0.23	–		0.907	0.337
	Opx	54.50	–	4.90	0.90	5.90	–	31.75	2.05	–	–	–		0.906	0.343
	Sp	0.18	0.17	37.66	32.76	9.30	0.32	19.50	0.10	–	–	–		0.789	0.879
A-15, 15, 1400	Gl	48.8	0.3	13.7	0.4	8.7	–	16.1	10.7	1.3	–	–	24.6	0.767	
	Ol	40.81	–	–	0.36	8.96	–	49.71	0.16	–	–	–		0.908	0.334
	Opx	54.78	–	4.57	1.13	5.60	–	32.05	1.87	–	–	–		0.911	0.323
	Sp	–	0.16	36.92	34.17	9.36	–	19.39	–	–	–	–		0.787	0.893
A-16, 15, 1425	Gl	48.9	0.3	12.8	0.5	9.0	–	17.5	9.9	1.1	–	–	29.1	0.776	
	Ol	40.40	–	0.23	0.32	8.72	–	50.17	0.16	–	–	–		0.911	0.338
A-51, 15, 1450	Gl	49.5	0.2	12.0	0.6	9.2	–	18.5	9.0	1.0	–	–	32	0.782	
	Ol	40.64	–	0.28	0.31	8.40	0.21	50.04	0.13	–	–	–		0.914	0.326
A-17, 20, 1415	Ol	40.32	–	0.22	0.17	9.45	–	49.65	0.19	–	–	–		0.904	
	Cpx	51.84	–	7.37	1.42	4.09	–	21.47	13.19	0.62	–	–		0.903	
	Sp	0.44	–	48.65	20.45	8.78	–	21.32	0.11	–	0.25	–		0.812	
A-18, 20, 1440	Gl	47.3	0.4	13.7	0.5	8.7	–	16.5	11.5	1.4	–	–	22.8	0.772	
	Ol	40.43	–	0.35	0.32	9.04	–	49.57	0.29	–	–	–		0.907	0.346
	Sp	0.28	–	41.71	28.53	9.14	–	20.20	–	–	–	0.14		0.798	0.858
A-19, 20, 1465	Gl	47.7	0.3	13.0	0.7	9.0	–	17.5	10.5	1.3	–	–	24.6	0.776	
	Ol	40.28	–	0.30	0.40	8.92	–	49.87	0.23	–	–	–		0.909	0.348
B-37, 7.5, 1260	Gl	50.4	0.6	16.2	0.2	6.6	–	10.7	13.2	2.1	–	–	20.5	0.743	
	Ol	40.65	–	–	0.15	9.50	–	49.45	0.24	–	–	–		0.903	0.311
	Cpx	51.90	0.30	6.11	1.20	3.24	–	16.95	19.60	0.70	–	–		0.903	0.310
	Sp	–	–	41.90	28.86	9.84	–	19.24	–	–	–	0.16		0.777	0.829
B-31, 7.5, 1280	Gl	50.6	0.5	15.1	0.2	7.0	–	11.6	13.1	1.9	–	–	22.6	0.747	
	Ol	40.52	–	0.20	0.16	9.27	–	49.43	0.18	–	0.24	–		0.905	0.311
	Sp	–	0.24	30.72	39.90	11.24	–	17.41	0.24	–	–	0.25		0.734	1.070
B-8, 7.5, 1300	Gl	50.8	0.5	14.0	0.3	7.2	–	12.6	12.9	1.7	–	–	25.3	0.757	
	Ol	40.79	–	–	0.23	8.94	0.21	49.67	0.16	–	–	–		0.908	0.315
	Sp	0.60	0.26	25.75	45.26	10.60	–	16.94	0.30	–	–	0.29		0.740	1.095
B-9, 7.5, 1310	Gl	51.0	0.4	13.1	0.3	7.5	–	13.5	12.7	1.5	–	–	28.7	0.762	
	Ol	40.79	–	–	0.25	8.82	–	49.98	0.16	–	–	–		0.910	0.318
	Sp	–	0.22	23.46	47.88	11.08	0.37	16.36	0.11	–	–	0.52		0.725	1.219

(*continued*)

Table 4 (*continued*)

Run, P(kb), T °C	Phase	SiO_2	TiO_2	Al_2O_3	Cr_2O_3	FeO	MnO	MgO	CaO	Na_2O	NiO	V_2O_3	F	mg	Kd
B-32, 7.5, 1325	Gl	51.2	0.4	12.5	0.4	7.7	–	14.1	12.3	1.4	–	–	30.7	0.765	
	Ol	40.71	–	0.19	0.30	8.59	–	49.96	0.25	–	–	–		0.912	0.315
	Sp	0.45	0.24	21.61	49.54	11.38	–	16.15	0.38	–	–	0.25		0.717	1.290
B-11, 7.5, 1350	Gl	51.5	0.3	11.3	0.6	8.3	–	15.8	11.0	1.2	–	–	35.8	0.772	
	Ol	40.96	–	–	0.41	8.35	–	50.11	–	–	0.17	–		0.915	0.317
B-15, 10, 1285	Gl	49.6	0.7	16.1	0.3	7.2	–	11.3	12.7	2.1	–	–	20.5	0.737	
	Ol	40.34	–	–	0.17	9.88	–	49.15	0.14	–	0.32	–		0.899	0.315
	Cpx	51.93	–	5.97	1.60	3.54	–	18.00	18.54	0.42	–	–		0.901	0.309
	Sp	0.18	–	43.73	25.84	9.50	0.27	19.89	–	–	0.36	0.23		0.789	0.750
B-38, 10, 1300	Gl	50.0	0.5	14.7	0.3	7.5	–	12.2	13.0	1.8	–	–	23.9	0.744	
	Ol	40.45	–	–	0.21	9.57	–	49.13	0.26	–	0.38	–		0.901	0.317
	Cpx	52.11	–	5.63	1.61	3.69	–	18.88	17.77	0.31	–	–		0.901	0.318
	Sp	0.13	0.25	39.63	30.14	10.06	–	19.17	0.20	–	0.24	0.18		0.773	0.854
B-34, 10, 1330	Gl	50.4	0.4	13.0	0.4	7.8	–	13.7	12.8	1.5	–	–	28.7	0.758	
	Ol	40.63	–	0.15	0.36	9.16	–	49.46	0.24	–	–	–		0.906	0.325
	Sp	0.13	0.19	24.71	47.41	10.78	–	16.32	0.13	–	–	0.33		0.730	1.160
B-17, 10, 1350	Gl	50.6	0.4	12.0	0.5	8.1	–	15.1	12.0	1.3	–	–	33.1	0.769	
	Ol	40.61	–	0.13	0.29	8.69	0.15	49.84	0.28	–	–	–		0.911	0.325
	Sp	0.16	0.26	21.24	50.68	10.69	–	16.21	0.16	–	0.28	0.32		0.730	1.229
B-36, 10, 1375	Gl	51.1	0.3	11.2	0.6	8.2	–	16.4	11.0	1.2	–	–	35.8	0.781	
	Ol	40.84	–	–	0.29	8.35	–	50.36	0.16	–	–	–		0.915	0.332
B-21, 15, 1350	Ol	40.46	–	0.15	0.34	9.44	0.16	48.87	0.26	–	0.32	–		0.902	
	Cpx	51.81	–	6.82	1.22	3.68	–	19.02	16.85	0.60	–	–		0.902	
	Sp	–	0.19	49.33	20.10	8.96	–	21.09	0.10	–	–	0.23		0.808	
B-22, 15, 1375	Ol	40.50	–	0.17	0.30	9.04	–	49.49	0.25	–	0.25	–		0.907	
	Cpx	52.75	–	5.29	1.78	3.98	–	21.09	14.70	0.41	–	–		0.904	
	Sp	0.20	0.17	34.26	35.97	9.86	0.34	18.45	0.22	–	0.27	0.26		0.769	
B-23, 15, 1400	Gl	49.0	0.5	12.1	0.5	8.2	–	16.1	12.2	1.4	–	–	30.7	0.778	
	Ol	40.70	–	0.22	0.29	8.55	–	49.72	0.25	–	0.27	–		0.912	0.338

The compositions are averages of 5–10 analyses recalculated to a total of 100 wt.% with all iron as FeO. *Interstitial melt. **Relic of starting orthopyroxene in the core of a large grain. *mg* $Mg/(Mg+Fe)$, $F = 100Na_2O^{bulk}/Na_2O^{glass}$ is estimated weight fraction of melt in run products. *Kd* $(Mg/Fe)^{mineral} : (Mg/Fe)^{melt}$

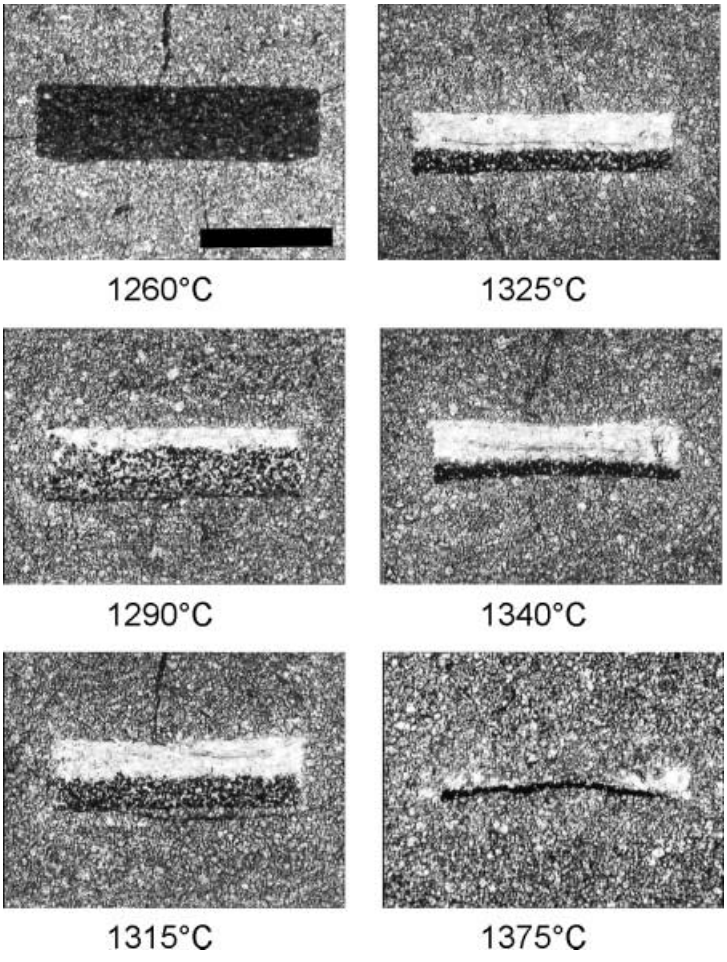

Fig. 2. Photomicrographs of experimental products obtained at 10 kbar and various temperatures (polished thin sections, transmitted light, the scale bar is 1 mm). Note the light dunitic halos around the central pyroxenite layer especially distinct at 1325 °C

shown in Fig. 4. SiO_2 decreases with increasing pressure and increases with temperature while contents are similar for 79/1 (Series A; more depleted) and ShT-1 (Series B; less depleted). A temperature increment of 20° corresponds to about 0.7 wt.% increase of MgO in the melt. At the same P–T conditions, the difference in MgO contents between the melts of Series A and B is only small (less than 0.7 wt.%) and FeO at the same P–T conditions is similar. The behaviour of CaO is more complex. Close to the solidus, CaO increases with increasing temperature with a maximum at clinopyroxene disappearance. The maximum abundance of CaO in both Series A and B experiments are very similar, despite the 1 wt.% CaO difference of the starting lherzolites. After clinopyroxene disappearance, CaO decreases with increasing temperature and melts of Series B are richer in CaO at the same T–P conditions. Na_2O contents are highest in the incipient melts and decrease with the increasing melt fraction. The Series B melts are richer in Na_2O than those of Series A at the same P–T conditions.

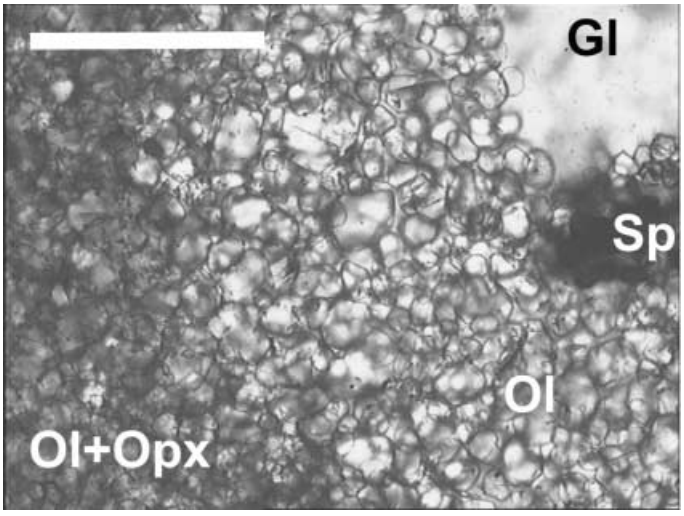

Fig. 3. Detail of an experimental sample (run A-14, 15 kbar, 1375 °C) illustrating zoning in the peridotite near the former spinel clinopyroxenite layer with the development of a dunitic halo. Polished thin section, transmitted light, the scale bar is 0.3 mm long

Al_2O_3 is lower in Series B, although alumina in the starting materials are almost identical. All the above features may be explained by higher melt fractions for Sample ShT-1 (Series B) at given T–P conditions. This and further differences in the lherzolite compositions determine the differences in melt compositions.

Compositions of crystalline phases

Olivine

Significant differences in olivine compositions from various zones were only detected in the experiment at 3.5 kbar and 1200 °C (mg# = 0.87 in the central zone and 0.89 in the lherzolite matrix). At all other conditions olivines were chemically uniform (mg# variations not more than 0.002). Forsterite increases with temperature and decreases with increasing pressure; Series A and B are similar at the similar P–T conditions.

Composition of olivine varies regularly with melt composition. The $K_D = (Fe/Mg)^{Ol} : (Fe/Mg)^{L}$ ranges from 0.294 to 0.348 and correlates positively with pressure and temperature. *Sobolev* and *Danyushevsky* (1994) argued that K_D depends primarily on temperature. Our data are approximated equally well by linear relationships with respect to pressure $K_D = 0.30 + 0.0025\,P(kbar)$ ($r^2 = 0.72$, $\sigma = 0.006$), which is similar to the expression given by *Takahashi* and *Kushiro* (1983) and *Ulmer* (1989), and temperature $K_D = 0.098 + 0.00017\,T(°C)$ ($r^2 = 0.74$, $\sigma = 0.006$). A somewhat better fit was obtained for the combined model: $K_D = 0.177 + 0.0001\,T(°C) + 0.0014\,P(kbar)$ ($r^2 = 0.84$, $\sigma = 0.005$). However, in the latter case, there is a strong correlation between coefficients at T and P ($r = -0.7$) owing to the correlation between the experimental P and T values.

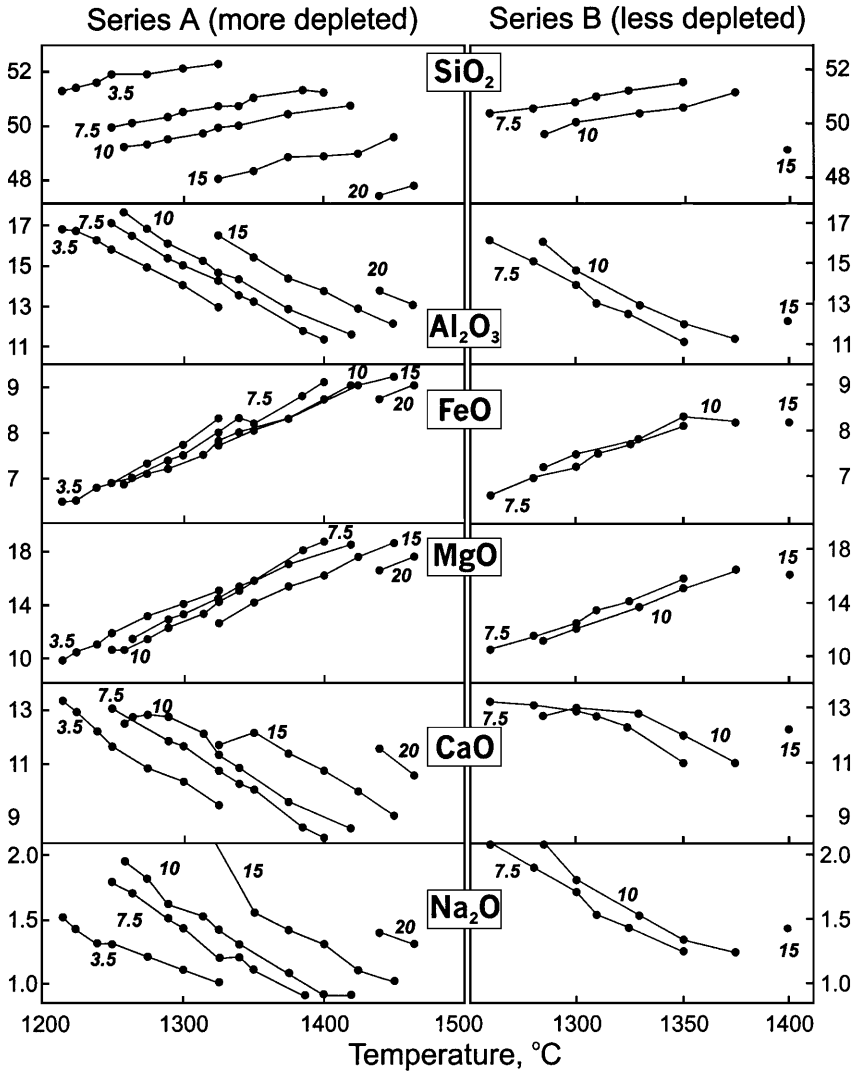

Fig. 4. Compositions of melts (wt.%) in the central melt pool as a function of temperature for Series A and B experiments. Numerals are experimental pressures in kilobars

Orthopyroxene

Orthopyroxenes are usually zoned. The cores sometimes contain relicts similar to the starting orthopyroxenes (Table 5, Run A-9). The difference in CaO and Al_2O_3 between core and rim may be up to 1.5–2.0 wt.%, and FeO and MgO only 0.5 and 1.0 wt.%, respectively. CaO contents in the newly-formed orthopyroxene is always higher than in the starting materials. $Mg/(Mg + Fe)$ of orthopyroxene is similar to that of olivine, consistent with the experiments on Mg–Fe distribution between the minerals (e.g. *von Seckendorf* and *O'Neill*, 1993; *Brey* and *Koehler*, 1991). K_D (Mg–Fe Opx-melt) varies from 0.24 to 0.33 and shows weak temperature dependence.

Al_2O_3 increases with increasing pressure and decreases with increasing temperature in the studied T–P range. With increasing temperature, CaO increases while clinopyroxene is present, and decreases after its disappearance. This behaviour is expected from subsolidus experiments of *Lindsley* and *Dixon* (1976) and *Nickel* and *Brey* (1984). Cr_2O_3 increases with temperature in accord with the results of *Jaques* and *Green* (1980), then decreases with increasing pressure.

Clinopyroxene

Clinopyroxenes are zoned to a similar extent as orthopyroxene. Differences between clinopyroxene compositions in the pyroxenite and lherzolite layers are random. Clinopyroxene from the central zone may be enriched or depleted in Na_2O compared to the lherzolite matrix. CaO and Al_2O_3 decrease with increasing temperature similar to results by *Jaques* and *Green* (1980), *Falloon* and *Green* (1987) and *Baker* and *Stolper* (1994).

The distribution coefficient of Fe and Mg between clinopyroxene and melt increases with temperature from 0.3–0.31 at 1250 °C to about 0.35 at 1400 °C. The alumina partition coefficient between clinopyroxene and liquid shows no systematic difference between experiments with different starting mixtures. Our results at 10 kbar are similar to other experimental values. D_{Na} in our experiments ranges from 0.17 to 0.23, which is slightly higher than the values from the majority of other experimental studies (e.g. *Putirka*, 1999). However, the scatter in measured Na_2O in glass is rather high and does not allow any definite inference on incomplete equilibration or sodium loss during microprobe analysis. Cr increases with temperature consistent with the data of *Jaques* and *Green* (1980) and *Falloon* and *Green* (1987).

Spinel

There is a range in spinel compositions in each charge, and spinel is zoned from core to rim. Spinel from the lherzolite matrix is systematically higher in Cr than in the central layer. Overall, Al_2O_3 decreases with temperature and Cr_2O_3 increases accordingly (see also *Jaques* and *Green*, 1980; *Falloon* and *Green*, 1987; *Baker* and *Stolper*, 1994) accompanied by an increase in FeO (*Engi*, 1983; *Dick* and *Bullen*, 1984). At the same P, T conditions, spinel from Series A is more magnesian and less chromian than the spinel from Series B. Near the solidus both spinels are similar. Chromium decreases with increasing pressure.

Discussion and conclusion

The experimental results demonstrate that the character of melting in a heterogeneous material differs substantially from that of homogenous peridotite of the same bulk composition. Most remarkable are the concentration of melt in the former pyroxenite at low temperature and low average melt fraction, the formation of a cumulate Ol-Sp layer and dunite around the central layer. Effects on mantle rheology and processes of melt extraction can be significant. For example, *Maaloe* (1998) demonstrated theoretically that source regions consisting of alternating melt

and residuum layers have permeabilities several orders of magnitude higher than percolative regions. The present experiments provide some constraints on such models.

Compositions of matrix peridotites and pyroxenite layers differ substantially from compositions studied by earlier authors but bulk sample compositions are similar to those of other studies concerned with melting of peridotite, e.g. MM-3 studied by *Baker* and *Stolper* (1994) and *Baker* et al. (1995) and KLB-1 studied by *Hirose* and *Kushiro* (1993). Figure 5 shows our melt compositions produced at 10 kbar compared with those of these authors. The results of heterogeneous and homogeneous source melting are quite similar. This implies that the combined result of a complex process including spinel clinopyroxenite melting and reaction of liquid with lherzolite is similar to that of simple lherzolite melting. Small differences may be readily explained by differences in starting composition.

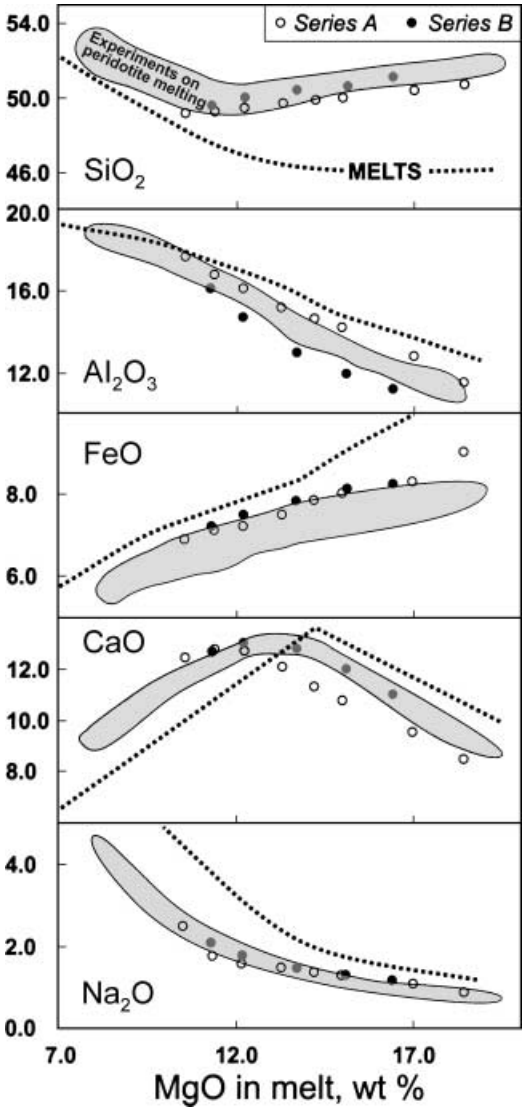

Fig. 5. Comparison of melt compositions from our experiments at 10 kbar with results of other workers on similar bulk peridotite compositions (*Baker* and *Stolper*, 1994; *Baker* et al., 1995; *Hirose* and *Kushiro*, 1993; *Falloon* et al., 1999, shaded areas) and with calculated compositions from MELTS (*Ghiorso* and *Sack*, 1995, dashed lines)

In particular, the lower FeO contents of *Baker* and *Stolper* (1994) and *Baker* et al. (1995) melts corresponds to the lower FeO content of peridotite sample MM-3 (7.18 wt.% FeO compared to 8 wt.% in our samples). The lower SiO_2 of our melts are almost within the analytical uncertainty, but it may be indicative of melt undersaturation with respect to orthopyroxene.

The compositions of melts formed from the clinopyroxene-spinel mixture are poorly known. They are constrained by the general reaction $Cpx + Sp = Liq + Ol$. We cannot characterise the reaction quantitatively, because our analyses represent melt compositions modified by interaction with the enclosing lherzolite. From this reaction, the melt formed by clinopyroxenite melting should be rich in CaO (no less than 15 wt.%) at the moment of complete Cpx dissolution. The melts derived from clinopyroxene-spinel mixture are undersaturated in orthopyroxene, which is suggested by the observed rapid orthopyroxene dissolution in the lherzolite matrix and the formation of the olivine + liquid reaction zone. The interstitial liquids are connected with the melt pool in the central zone and its composition changes via diffusion and approaches equilibrium with the bulk lherzolite. At high temperature, clinopyroxene disappears from the central layer and the reaction zone. Subsequent melting involves olivine and spinel dissolution in the central zone. The high initial Cr_2O_3 content in the spinel clinopyroxenite (Table 3) resulted in the concentration of spinel in the central zone (Fig. 2).

Undersaturation with orthopyroxene in the central layer provided high melt reactivity and its rapid exchange between the matrix and melt pool. The degree of undersaturation is probably pressure dependent. For example, *Yaxley* and *Green* (1998) observed orthopyroxene as a reaction product when melting eclogite at 35 kbar. However, we did not observe orthopyroxene formation as a reaction product at pressures up to 20 kbar. In cases where the melt is closer to equilibrium with the surrounding peridotite, the reaction may result only in the formation of thin diffusion zones in peridotite minerals in contact with melt. Pervasive melt interaction may be hindered if newly-formed pyroxene selvages are formed between melt and peridotite. Such relationships were documented in xenoliths from La Palma by *Kluegel* (1998). These observations suggest that the formation of infiltration zones in peridotite is not an ubiquitous process and occurs only if the melt is undersaturated in orthopyroxene.

Hirschmann and *Stolper* (1996) proposed melting of a mantle containing garnet pyroxenite veins to account for the ''garnet signature'' in MORB. Their model includes early melting of pyroxenite veins with garnet retention in the solid residue under conditions, when garnet is not stable in the peridotite material. Our results suggests that such a scenario is possible only under certain conditions. We did not observe garnet in our experiments even at 20 kbar, although *Hirschmann* and *Stolper* (1996) predicted garnet clinopyroxenite to be stable at pressure down to 14 kbar. The Cr/Al ratio in the initial spinel clinopyroxenite was not very high (Table 3) and the absence of garnet in the experimental products could result from its rapid dissolution. Reaction melt infiltration greatly facilitates equilibration of melt with the enclosing lherzolite. Thus, garnet in partially molten pyroxenite melt will be dissolved much more rapidly than in the case of garnet pyroxenite melting. The size of pyroxenite zones is critical for the model of *Hirschmann* and *Stolper* (1996). In our experiments, equilibration of millimetre-sized melt pocket took

about 10 hours. If diffusion of components in melt is the controlling factor, the time necessary for equilibration is approximately proportional to the square of the linear size. Thus, the interaction of a melt pocket about 10 cm in size would require ca. 10 yr. The formation of a ''garnet signature'' by the mechanism of veined mantle melting is probably plausible for large (tens to hundreds meters) heterogeneities in the mantle. This conclusion is in agreement with the numeric modelling by *Richter* and *Daly* (1989), who demonstrated that melting of a heterogeneous mantle source produces a solitary wave, which is capable of transporting large amounts of melt but does not carry any anomalous geochemical properties related to a heterogeneity much smaller than the melting region.

It should be noted that the application of the present result to natural parageneses has certain limitations. First, our experiments concerns the situation when both pyroxenite and lherzolite are above solidus. Moreover, melt fraction in the lherzolite matrix was probably high in the majority of our experiments. *Hirschmann* and *Stolper* (1996) suggested that garnet pyroxenite could melt when lherzolite was still below the solidus. Then, equilibration with the lherzolite would require much longer time intervals. Second, we studied only the behaviour of major components, and the effect on trace elements and isotope signatures can be different. Third, the processes occurring at the melting of heterogeneous mantle material may be diverse. For example, *Yaxley* and *Green* (1998) performed experiments on the melting of eclogite (Cpx + Grt + coesite) in a lherzolite matrix at 35 kbar. The early melt derived in the eclogite layer was dacitic and its reaction with the lherzolite resulted in orthopyroxene crystallisation and produced garnet-clinopyroxene residue.

The present results suggest a possible mechanism for the formation of dunite bodies in the mantle. Dunites frequently occur as xenoliths in alkali basalts and as larger bodies in ophiolites (*Quick*, 1981; *Kelemen*, 1990). *Kelemen* (1990) suggested that such dunites are products of the interaction of fractionating basalt magma with the wall harzburgite. Our experiments show that similar rocks may form by the melting of a heterogeneous material including pyroxenite layers. *Suhr* (1999) described along-strike clinopyroxenite to dunite transition in ophiolitic massifs. Such relationships could result from a process similar to that modelled in our experiments.

Acknowledgements

We are grateful to *Ch. Ballhaus*, *L. Danyushevsky* and *G. Suhr* for their suggestions and critical reading of the manuscript. The work was partially supported by the Russian Foundation for Basic Research and Deutsche Forschungsgemeinschaft.

References

Allegre CJ, *Turcotte DL* (1986) Implications of a two component marble-cake mantle. Nature 323: 123–126

Baker MB, *Stolper E* (1994) Determining the composition of high-pressure mantle melts using diamond aggregates. Geochim Cosmochim Acta 58: 2811–2827

Baker MB, *Hirschmann MM*, *Ghiorso MS*, *Stolper EM* (1995) Compositions of near-solidus peridotite melts from experiments and thermodynamic calculations. Nature 375: 308–311

Bodiner JL, *Guiraud M*, *Fabries J*, *Dostal J*, *Dupuy C* (1987) Petrogenesis of layered pyroxenites from the Lherz, Freychinede and Prades ultramafic bodies (Ariege, French Pyrenees). Geochim Cosmochim Acta 51: 279–290

Brey GP, *Koehler T* (1990) Geothermometry in four-phase lherzolites. II. New thermobarometers and practical assessment of existing thermobarometers. J Petrol 31: 1353–1378

Bulatov VK (1990) A high-temperature salt cell for a piston-cylinder apparatus. Geochem Int 1: 95–101

Campbell IH (1998) The mantle's chemical structure: insights from the melting products of mantle plumes. In: *Jackson I* (ed) The Earth's mantle: composition, structure, and evolution. Cambridge University Press, Cambridge, pp 259–310

Dick HJB, *Bullen T* (1984) Chromian spinel as a petrogenetic indicator in abyssal and alpine-type and spatially associated lavas. Contrib Mineral Petrol 86: 54–76

Engi M (1983) Equilibria involving Al–Cr spinel: Mg–Fe exchange with olivine. Experiments, thermodynamic analysis, and consequences for geothermometry. Am J Sci 283-A: 29–71

Falloon TJ, *Danyushevsky LV* (2000) Melting of refractory mantle at 1.5, 2 and 2.5 GPa under anhydrous and H_2O-undersaturated conditions: implications for the petrogenesis of high-Ca boninites and the influence of subduction component on mantle melting. J Petrol 41: 257–283

Falloon TJ, *Green DH* (1987) Anhydrous partial melting of MORB pyrolite and other peridotite compositions at 10 kbar: implications for the origin of primitive MORB glasses. Mineral Petrol 37: 181–219

Falloon TJ, *Green DH* (1988) Anhydrous partial melting of peridotite from 8 to 35 kbars and the petrogenesis of MORB. J Petrol (Special Lithosphere Issue): 379–414

Falloon TJ, *Green DH*, *Danyushevsky LV*, *Faul UH* (1999) Peridotite melting at 1.0 and 1.5 GPa: an experimental evaluation of techniques using diamond aggregates and mineral mixes for determination of near-solidus melts. J Petrol 40: 1343–1375

Ford CE, *Russell DG*, *Groven JA*, *Fisk MR* (1983) Distribution coefficients of Mg^{2+}, Fe^{2+}, Ca^{2+} and Mn^{2+} between olivine and melt. J Petrol 24: 256–265

Fujii T, *Scarfe CM* (1985) Composition of liquids coexisting with spinel lherzolite at 10 kbar and the genesis of MORBs. Contrib Mineral Petrol 90: 18–28

Ghiorso MS, *Sack RO* (1995) Chemical mass transfer in magmatic processes. IV. A revised and internally consistent thermodynamic model for the interpolation and extrapolation of liquid-solid equilibria in magmatic systems at elevated temperatures and pressures. Contrib Mineral Petrol 119: 197–212

Hirschmann MM, *Stolper EM* (1996) A possible role for garnet pyroxenite in the origin of the ''garnet signature'' in MORB. Contrib Mineral Petrol 124: 185–208

Hirose K, *Kushiro I* (1993) Partial melting of dry peridotites at high pressures: determination of compositions of melts segregated from peridotite using aggregates of diamond. Earth Planet Sci Lett 114: 477–489

Holloway JR, *Pan V*, *Gudmunsson G* (1992) High-pressure fluid absent melting experiments in the presence of graphite: oxygen fugacity, ferric/ferrous ratio and dissolved CO_2. Eur J Mineral 4: 105–114

Irving AJ (1980) Petrology and geochemistry of composite ultramafic xenoliths in alkalic basalts and implications for magmatic processes within the mantle. Am J Sci 280-A: 389–426

Ito K, *Kennedy GC* (1967) Melting and phase relations in a natural peridotite to 40 kbars. Am J Sci 265: 519–539

Jackson ED, *Wright TL* (1970) Xenoliths in the Honolulu volcanic series. J Petrol 11: 405–430

Jaques AL, *Green DH* (1980) Anhydrous melting of peridotite at 0–15 kb pressure and the genesis of tholeiitic basalts. Contrib Mineral Petrol 73: 287–310

Johnson KT, *Kushiro I* (1992) Segregation of high-pressure partial melts from peridotite using aggregates of diamonds: a new experimental approach. Geophys Res Lett 19: 1703–1706

Jousselin D, *Mainprice D* (1998) Melt topology and seismic anisotropy in mantle peridotites of the Oman ophiolite. Earth Planet Sci Lett 164: 553–568

Kelemen PB (1990) Reaction between ultramafic rocks and fractionating basaltic magma. I. Phase relations, the origin of calc-alkaline magma series, and the formation of discordant dunite. J Petrol 31: 51–98

Kellogg LH, *Turcott DL* (1990) Mixing and the distribution of heterogeneities in a chaotically convecting mantle. J Geophys Res 95: 421–432

Kluegel A (1998) Reaction between mantle xenoliths and host magma beneath La Palma (Canary Islands): constraints on magma ascent rates and crustal reservoirs. Contrib Mineral Petrol 131: 237–257

Kornprobst J (1969) Le massif ultrabasique des Beni Bouchera (Rif Interne, Maroc): Etude des peridotites de haute temperature et de haute pression, et des pyroxenolites, a grenat ou sans grenat, qui leur sont associees. Contrib Mineral Petrol 23: 283–322

Kumar N, *Reisberg L*, *Zindler A* (1996) A major and trace element and strontium, neodymium, and osmium isotopic study of a thick pyroxenite layer from the Beni Bousera Ultramafic Complex of northern Morocco. Geochim Cosmochim Acta 60: 1429–1444

Langmuir CH, *Bender JF*, *Bence AE*, *Hanson GN* (1977) Petrogenesis of basalts from the FAMOUS area: Mid-Atlantic Ridge. Earth Planet Sci Lett 36: 133–156

Langmuir CH, *Klein EM*, *Plank T* (1992) Petrological systematics of mid-ocean ridge basalts: constraint on melt migration beneath ocean ridges. Geophys Monogr Am Geophys Union 71: 183–280

Lindsley DH, *Dixon SA* (1976) Diopside-enstatite equilibria at 850 to 1400 °C, 5 to 35 kbars. Am J Sci 276: 1285–1301

Maaloe S (1998) Melt dynamics of a layered mantle plume source. Contrib Mineral Petrol 133: 83–95

Nickel K, *Brey G* (1984) Subsolidus orthopyroxene-clinopyroxene systematics in the system CaO–MgO–SiO_2 to 60 kb: a reevaluation of the regular solution model. Contrib Mineral Petrol 87: 35–42

Nielsen RL, *Gallahan WE*, *Newberger F* (1992) Experimentally determined mineral-melt partition coefficients for Sc, Y and REE for olivine, orthopyroxene, pigeonite, magnetite and ilmenite. Contrib Mineral Petrol 110: 488–499

O'Hara MJ (1985) Importance of the shape of the melting regime during partial melting of the mantle. Nature 314: 58–62

Plank T, *Langmuir CH* (1992) Effects of the melting regime on the composition of the oceanic crust. J Geophys Res 97: 19749–19770

Press S, *Witt G*, *Seck HA*, *Eonov DA*, *Kovalenko VI* (1986) Spinel peridotite xenoliths from the Tariat depression, Mongolia. I. Major element chemistry and mineralogy of a primitive mantle xenolith suite. Geochim Cosmochim Acta 50: 2587–2599

Putirka K (1999) Clinopyroxene + liquid equilibria to 100 kbar and 2450 K. Contrib Mineral Petrol 135: 151–163

Quick JE (1981) The origin and significance of large tabular dunite bodies in the Trinity peridotite, Northern California. Contrib Mineral Petrol 78: 413–422

Reed SJB, *Ware NG* (1975) Quantitative electron microprobe analysis of silicates using energy-dispersive X-ray spectrometry. J Petrol 16: 499–519

Richter FM, *Daly SF* (1989) Dynamical and chemical effects of melting a heterogeneous source. J Geophys Res 94: 12499–12510

Sautter V, *Fabries J* (1990) Cooling kinetics of garnet websterites from the Freychinede orogenic lherzolite massif, French Pyrenees. Contrib Mineral Petrol 105: 533–549

Sen G (1982) Composition of basaltic liquids generated from a partially depleted lherzolite at 9 kbar pressure. Nature 299: 336–338

Sen G (1988) Petrogenesis of spinel lherzolite and pyroxenite suite xenoliths from the Koolau shield, Oahu, Hawaii: implications for petrology of the post-eruptive lithosphere beneath Oahu. Contrib Mineral Petrol 100: 61–91

Sobolev AV, *Danyushevsky LV* (1994) Petrology and geochemistry of boninites from the northern termination of the Tonga Trench: constraints on the generation conditions of primary high-Ca boninite magmas. J Petrol 35: 1183–1211

Stolper E (1980) A phase diagram for mid-ocean ridge basalts: preliminary results and implications for petrogenesis. Contrib Mineral Petrol 74: 13–27

Suhr G (1999) Melt migration under oceanic ridges: inferences from reactive transport modelling of upper mantle hosted dunites. J Petrol 40: 575–599

Takahashi E, *Kushiro I* (1983) Melting of a dry peridotite at high pressures and basalt magma genesis. Am Mineral 68: 859–879

Thompson RN, *Kushiro I* (1972) The oxygen fugacity within graphite capsules in the piston cylinder apparatus at high pressures. Carnegie Inst Washington Yearb 71: 615–616

Ulmer P (1989) The dependence of the Fe^{2+}–Mg cation-partitioning between olivine and basaltic liquid on pressure, temperature and composition. An experimental study to 30 kbars. Contrib Mineral Petrol 101: 261–273

von Seckendorff V, *O'Neill HSC* (1993) An experimental study of Fe–Mg partitioning between olivine and orthopyroxene at 1173, 1273 and 1423 K and 1.6 GPa. Contrib Mineral Petrol 113: 196–207

Witt G, *Seck HA* (1987) Temperature history of sheared mantle xenoliths from the West Eifel, West Germany: evidence for mantle diapirism beneath the Rhenish Massif. J Petrol 28: 475–493

Yaxley GM, *Green DH* (1998) Reactions between eclogite and peridotite: mantle refertilisation by subduction of oceanic crust. Schweiz Mineral Petrogr Mitt 78: 243–255

Yang H-J, *Sen G*, *Shimizu N* (1998) Mid-ocean ridge melting: constraints from lithospheric xenoliths at Oahu, Hawaii. J Petrol 39: 277–295

Authors' addresses: *V. K. Bulatov*, Vernadsky Institute of Geochemistry and Analytical Chemistry, Russian Academy of Sciences, ul. Kosygina 19, Moscow, 117975 Russia; *A. V. Girnis*, Institute of the Geology of Ore Deposits, Petrography, Mineralogy and Geochemistry, Russian Academy of Sciences, Staromonetny per. 35, Moscow, 109017 Russia; *G. P. Brey*, Institut für Mineralogie, J. W. Goethe-Universität Frankfurt, Senckenberganlage 28, D-60054 Frankfurt/M, Federal Republic of Germany